ISTITUTO NAZIONALE DI FISICA NUCLEARE

Sezione di Catania

INFN/BE-96/04
17 Settembre 1996

A. Sibirtsev:

SUBTHRESHOLD PION PRODUCTION FROM PROTON-NUCLEUS COLLISIONS

PACS: 25.70.z

SIS-Pubblicazioni
dei Laboratori Nazionali di Frascati

INFN – Istituto Nazionale di Fisica Nucelare
Sezione di Catania

INFN/BE-96/04
17 Settembre 1996

SUBTHRESHOLD PION PRODUCTION FROM PROTON–NUCLEUS COLLISIONS*

A. Sibirtsev†
INFN–Sezione di Catania, Department of Physics, University of Catania, Corso Italia 57,
I–95129 Catania (Italy)

Abstract

Pion production from $p + A$ collisions at energies below and above the reaction threshold in free space was studied within the impulse approximation. The model fairly well reproduced the energy and angular spectra for the positive pions, while underestimate the π^--production cross sections. The discrepancy is not related to the beam energy and thus is not influenced by the subthreshold phenomena. We discuss the contribution from the secondary interactions as the charge-exchange scattering which might populate the negative pion production.

*Supported in part by Istituto Nazionale di Fisica Nucleare, Sezione di Catania and Physics Department of University of Catania

†Permanent address: Laboratory of Nuclear Problems, Joint Institute of Nuclear Research, Dubna, 141980, Russia

where T_{th} stands for the projectile kinetic energy in the laboratory, while m_π, M_B and M_A are the pion, projectile and the target masses respectively.

The threshold for neutral pion production in free proton-proton collision equals to 279.6 MeV. For the proton-nucleus collision the absolute kinematical threshold ranges from the free pion mass (for heavy target) to the free NN threshold. The most surprising experimental finding was the observation of sizeable pion yields from $Kr + Zr$ collisions at such a low energy as 20 MeV/u [5, 6]. However note, that the absolute threshold for such a system is around 3 MeV/u.

The simple kinematical relation (2) is based on the coherent pion production, i.e. when the colliding systems interact as a two pointed objects. Within the Glauber formalism one can slice such interaction into N-body terms. For instance the proton-nucleus collision may be presented as

$$p + A := N_1\{p + N\} + N_2\{p + NN\} + N_3\{p + 3N\} + ... = \sum_{j=1}^{A} N_j\{p + jN\} \quad (3)$$

where N_j stands for the effective collision number [7]

$$N_j = \frac{1}{j!} \int d^2b \ \exp\left[-\sigma T(b)\right][T(b)]^j \quad (4)$$

with the profile function

$$T(b) = \int dz \ \rho(b, z), \quad (5)$$

where $\rho(\mathbf{r})$ is the nuclear density distribution and σ stands for the NN total cross section.

Each term of the row (3) refers to certain reaction threshold in accordance with the definition (2). Thus one can conclude that the pion production below free NN threshold is related with the collective phenomena or the many body collisions.

However the system of a bound nucleons possess the Fermi motion and the point is that the internal momentum of the nucleus permits the pion production below free $N + N$ threshold.

As was shown by Bertsch [8] the Fermi motion permits the pion production from heavy ion collisions at such low energy as $\simeq$ 54 MeV/u. The combination of the internal momenta of the colliding nuclei gives enough energy to produce the pion at even low energies, but the reaction is blocked by the Pauli principles.

Within present approach we analyze the subthreshold pion production from $p+A$ collisions due to the Fermi motion.

3 Elementary production cross sections.

In free space and at bombarding energies below 1 GeV the pions are produced from the following reactions

$$p + N \rightarrow N + N + \pi \quad (6)$$

and

$$p + N \rightarrow d + \pi \quad (7)$$

At low energies the produced np pair has small relative momentum and its wave function strongly overlaps with the deuteron wave function. Fig.1 demonstrates that the deuteron channel is dominant for the pion production at energies close to the reaction threshold.

The direct observation of the kinematical peak from $p+N \to d+\pi$ reaction was reported from the experimental study of the fast deuteron production at forward angles from $p+A$ collisions [14].

The analysis of the quasifree subthreshold pion production in the reaction $^{12}C(p,d\pi^+)^{11}B$ at beam energy of 223 MeV also illustrates that the reaction mechanism is related to the elementary reaction $p+p \to d+\pi^+$ [15].

Second, the cross section of π^--production from pN interactions is substantially smaller those for π^+ and π^0-meson. Therefore the secondary interactions of the pions in the nuclear matter like

$$\pi^0 + n \to \pi^- + p \tag{10}$$

become important as an additional source of π^--production [16]. The charge-exchange cross section is around 15-30% of the total one at pion momenta below 1 GeV. It means that the contribution to π^--meson production from the primary pN collisions is comparable to those from the secondary charge-exchange scattering (10).

4 The model.

In terms of a multiple scattering theory the proton-nucleus collision can be expressed as a sum of the two-body interactions [17, 18, 19] shown in Fig.2. These graphs presents a microscopic determination of (3).

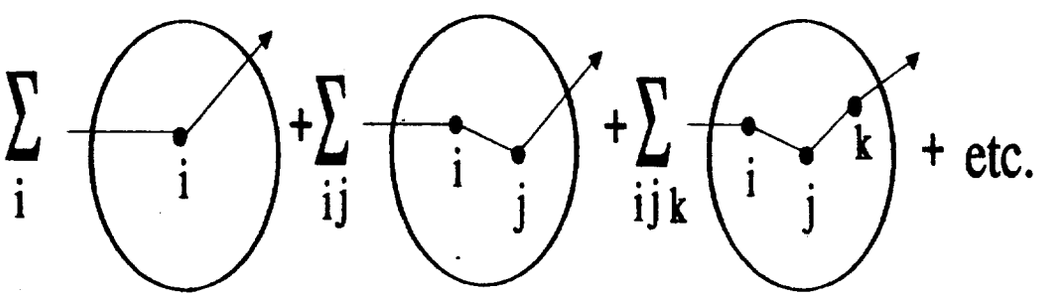

Figure 2: Graphical presentation of the multiple scattering theory.

The individual interactions differ from the nucleon-nucleon collisions in free space, because the reaction occurs in a surrounding of other target nucleons. The system of a bound nucleons influences the NN collisions through the Pauli principle and Fermi motion as well as the effective nuclear potential or the mean field effects [20].

Taking into consideration only the first term from the multiple scattering theory one get the single scattering approximation, which we refer as the direct production mechanism.

At low energies the π-meson inclusive spectrum from the isobar model is roughly similar to those from the three body final state phase space or s-wave production. The pion spectrum from Δ-excitation at incident energies above around 1 GeV shows the high energy tail, while those from s-wave calculation does not [30, 24].

The deuteron channel was calculated as follows [31]. We determine the deuteron density as

$$\rho_d(p_d) = \int d^3q \Phi_d(q) H_{np}(q, p_d) \qquad (15)$$

where $\Phi_d(q)$ is the squared deuteron wave function and H_{np} stands for the two-particle density matrix of the neutron-proton states with the total momentum p_d and relative momentum $2q$ [33]. The deuteron wave function for the Bonn potential [32] was adopted. The density matrix was calculated with the isobar model described above. The deuteron cross section should be corrected by the effective final state NN interaction similar to [34], which enhanced the production near the reaction threshold. We adopt a phenomenological way and renormalize the deuteron density ρ_d with the elementary cross section of the reaction (7).

The coalescence mechanism simulates quasi-two-body final state, which indicates the pion as well as the deuteron kinematical peak in the differential cross sections. Within sophisticated approach the deuteron channel can be calculated directly as in the reaction $p + N \to d + \pi$, similar to [11]. However it rises the problem concerning the deuteron existence in the nuclear medium. The deuteron radius is larger the average distance between the nuclear nucleons, so in principle it can not be formed inside the nucleus. The coalescence model [35] assumes the deuteron formation outside the target or at the nuclear surface.

Note that pion and deuteron spectra calculated with the coalescence mechanism differ from those obtained with the direct production (7) due to the reaction blocking by the Pauli principles and non sharp deuteron wave function in Eq.15.

5 Effective collision number and pion reabsorption.

5.1 Factor N_{eff}.

The factor $N_{eff}(E_\pi)$ in Eq.(11) is accounting both for the A-dependence of the Δ-resonance production and the final stage of the pion interaction in nuclear medium.

Similar to [36, 37], the effective collision number was calculated as

$$N_{eff} = \int_0^{+\infty} bdb \int_{-\infty}^{+\infty} \rho(b,z)dz \int_0^{2\pi} d\phi \times \left[exp\left(-\sigma_{tot}(pN) \int_{-\infty}^{z} \rho(b,\xi)d\xi - \sigma_{tot}(\pi N, E_\pi) \int_0^{+\infty} \rho(\mathbf{r}[\zeta])d\zeta \right) \right], \qquad (16)$$

where $\rho(r)$ is the one-particle density distribution taken from [38] and normalized to the target mass number A. $\mathbf{r}[\zeta]$ appearing in eq.(16) is defined as

$$\mathbf{r}[\zeta] = \mathbf{r}_0(b, 0, z) + \zeta\, \hat{\mathbf{e}}, \qquad (17)$$

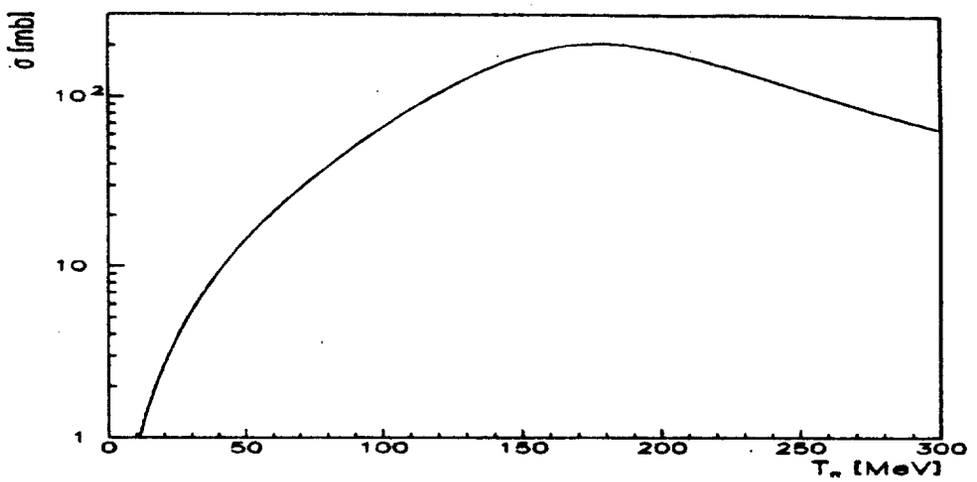

Figure 3: $\pi^+ + p$ cross section as a function of the pion kinetic energy.

where b and z stand for the impact parameter and the z-component of the coordinate along the beam-axis, respectively. Here $\hat{\mathbf{e}}$ is a unit vector in coordinate space defined as

$$\hat{\mathbf{e}} := (sin\theta cos\phi, sin\theta sin\phi, cos\theta) \tag{18}$$

with θ being the pion emission angle in the laboratory system. Moreover $\sigma_{tot}(pN)$ stands for the total $p + N$ cross section, while $\sigma_{tot}(\pi N)$ is the $\pi + N$ cross section. We account for the N_{eff} dependence on the $\pi + N$ cross section shown in Fig.3, because of the strong energy dependence of the $\sigma_{tot}(pN)$.

The effective collision numbers (16) calculated for C, Ni and Cu-target are shown in Fig.4,5 as a function of the pion emission angle and for several πN cross sections. Note that our collisions numbers growth around 1.5-2 times with increasing of the emission angle from 0^0 to 180^o. Moreover the effective collision numbers reduce almost twice when the $\pi + N$ cross section ranging from 20 to 100 mb.

The standard way [39, 40, 41] to account for the particle final state interaction (FSI) in $p + A$ and $A + A$ collisions is to multiply the production cross section by the factor

$$\kappa(E_\pi, A) = exp[-L_A/\lambda_\pi(E_\pi)] \tag{19}$$

where L_A is the radius of the interaction zone, i.e. the distance passed by the pion in nuclear medium, which is frequently taken equal to the nuclear radius. λ_π stands for the mean free path of the pion as

$$\lambda_\pi{}^{-1} = \rho_0 \times \sigma_{in}(\pi N) \tag{20}$$

where ρ_0 is average nuclear density and $\sigma_{in}(\pi N)$ is the inelastic cross section of $\pi + N$ interaction.

The factor (19) substantially depends on the target mass A as well as on the $\pi + N$ cross section. For instance for the copper the factor κ changes from $\simeq$0.2 to $\simeq$0.0005 when the cross section varying from 20 to 100 mb. Let us to remind that within our approach the reabsorption is not such strong.

Another sophisticated ways to account for the final state interaction are discussed in [42]. Similar to (19) those approximations are just simplification of the Glauber

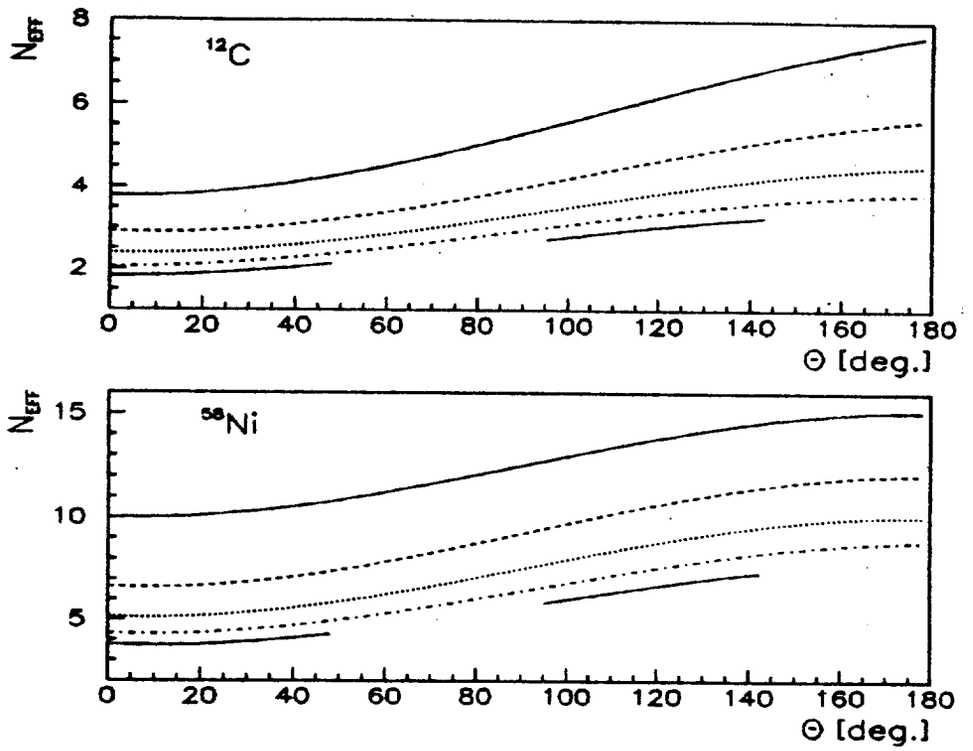

Figure 4: Effective collision number as a function of the pion emission angle θ calculated for: a) $p + C$ and b) $p + Ni$ collisions and for $\pi + N$ cross section of 20 -solid, 40 -dashed, 60 -dotted, 80 -dashed-dotted and 100 mb -long dashed-dotted line.

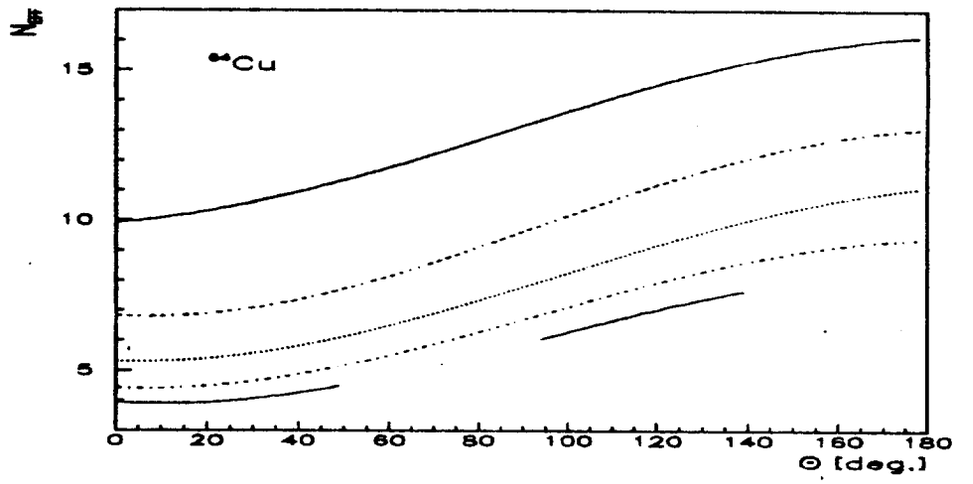

Figure 5: Similar as in Fig.4 for $p + Cu$ collisions.

formula (16) and substantially overestimates the FSI for strong interacting particles, like pions, K^--mesons, antiprotons, etc.

Within the calculations of K^+-meson production [43, 44], the factor N_{eff} was

obtained by the Glauber approach but does not account for the K^+-meson interaction. The total cross section for the K^+N-interaction is small $\sigma(KN) \simeq 12mb$, thus one can treat it perturbatively and get the effective collision number for $\sigma(KN)$ from the results performed in Fig.4,5.

Neglecting the FSI, that is reasonable for the weak interacting particles like K^+-mesons, the effective collision numbers from [43, 44] were parameterized as

$$N_{eff} = A^{0.75\pm0.01}. \tag{21}$$

which indicates reasonable agreement with present results for small $\sigma_{tot}(\pi N)$.

Note that the A-dependence from (21) is very close to those from the experimental data on π^o-meson production from $p + A$ collisions at 200 MeV [45].

5.2 Pion absorption and scattering.

The target effect reveals the dramatic importance of final state interaction of the pions in the residual nuclear environment. The analysis on experimental data on π^+ and π^--production in heavy ion collisions results the average pion absorption length of about 6-7 fm [48]. By the other hand the analysis of the experimental data on direct pion reabsorption in π+A collision results the absorption length of about 3 fm at the same pion energies.

However let us to emphasize that within our approach the factor N_{eff} accounts for the distortion of the primary pion spectra. We do not distinguish between the pion elastic or inelastic rescattering and the pion reabsorption as (13). Moreover we prevent from using the formula (19) to account the pion absorption in nuclear matter.

Indeed the meaning of Eq.16 concerning the FSI is to account for the probability that directly produced pions interact in nucleus changing their emission angle. It does not matter, is the interaction due to the $\pi + N \to \pi + N$ scattering or because of the real reabsorption (13). Moreover the pion scattering populates the angles differ from the primary emission angles and are relayed as secondary interactions.

To account for the pion reabsorption one needs to incorporate the cross section of reaction (13) [46, 47] instead of $\sigma_{tot}(\pi N)$ from Eq.16 as well as to make similar with Eq.19.

6 Nucleon momentum distribution.

The function $\Phi(q)$ appearing in Eq.11 stands for the internal nucleon momentum distribution. In the noninteracting Fermi-gas model the occupation probability of states with momentum q is

$$\Phi(q) = \frac{3}{4\pi q_F^{3/2}} \Theta(q_F - q) \tag{22}$$

with q_F being the Fermi momentum

$$q_F = \left[\frac{3}{2}\,\pi^2\,\rho_0\right]^{1/3} \simeq 263 MeV/c \tag{23}$$

where $\rho_0 = 0.16\ fm^{-3}$ is the average nuclear density. The corresponding Fermi energy ${q_F}^2/2m_N$, with m_N being the mass of free nucleon, is maximal kinetic energy of a neutron bound in the nucleus. The binding energy of the last nucleons is roughly 8 MeV. Thus the minimal total energy of the stuck nucleon must be $\simeq m_N - 35$ MeV [49]

Short range NN interactions induce correlations in the wave function, which deplete states below the Fermi sea and make the states above the Fermi level partially occupied [50, 51]. Thus the nuclear momentum distribution $\Phi(q)$ has a tail at $q > q_F$.

Moreover the particles in nuclear matter have not precise energies. The relation between the momentum of the particle and its energy is defined by the spectral function $P(q, E)$. The spectral function gives the joint probability of finding the nuclear nucleon with momentum q and removal energy E. However the evaluation of $P(q, E)$ is a hard problem [52, 53, 54, 55, 56].

If no reliable spectral function is available we may use an approximation, which correlated the momentum distribution

$$\Phi(q) = \int dE\ P(q, E) \tag{24}$$

with the mean removal energy $\langle E \rangle$ defined as

$$\langle E \rangle = \int d^3q\ dE\ E\ P(q, E) \tag{25}$$

As was pointed out by Fernandez de Cordoba et al. [57] this approximation is quite accurate when one do not explore the momenta significantly larger q_F.

In accordance with the Koltun sum rule [58] the binding energy per nucleon ϵ is related with the mean removal energy $\langle E \rangle$ as

$$2\epsilon = \frac{A-2}{A-1}\langle T \rangle - \langle E \rangle \tag{26}$$

where A is the target atomic number and $\langle T \rangle$ stands for the mean single-particle kinetic energy,

$$\langle T \rangle = \int_0^{q_{max}} d^3q\ \frac{q^2}{2m}\ \Phi(q) \tag{27}$$

with $q_{max} = \infty$.

Although the spectral function is not observable quantity, the energy sum rule describes it with the measurable binding energy ϵ and the mean kinetic energy, because $\Phi(q)$ might be obtained from the analysis of the properties of single-particle states in nuclei with the experimental data [59, 60].

When the distribution (24) does not contain the high momentum component generated by the short-range and tensor correlations, the mean kinetic energy (27) is that as obtained with the mean field approach. Taking the Gaussian momentum distribution as

$$\Phi(q) = (2\pi)^{-3/2}\ \alpha^{-3}\ exp\left(-q^2/2\alpha^2\right) \tag{28}$$

with the slope α ranging from 139 to 151 MeV/c for ^{12}C and ^{208}Pb nuclei respectively [61] one can get the mean removal energy equals almost 40 MeV.

Fig.6 shows the mean removal energy as function of the momentum q_{max}. Here $\langle E \rangle$ was calculated with q_{max} being the upper limit of the integration in Eq.27 and

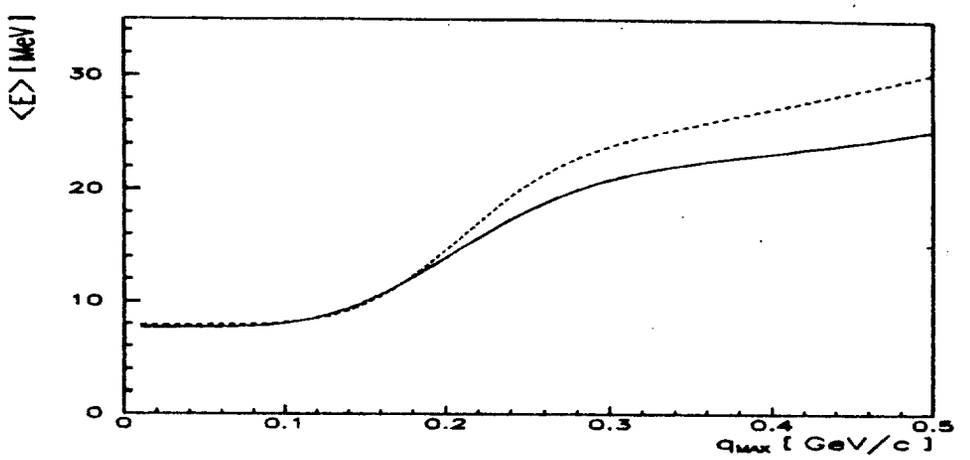

Figure 6: Dependence of mean removal energy on maximal nuclear momentum calculated for for carbon -solid and lead -dashed line.

the parametrizations of the nucleon momentum distributions $\Phi(q)$, which are shown in Fig.7 and were taken from Ciofi degli Atti and Simula [61]. Note that the high momenta of the distribution $\Phi(q)$ are related with the high removal energies, as is illustrated with Fig.6.

The relation between the high momentum and high removal energy components has been for the first time illustrated in [62] considering the saturation of the momentum sum rule (24). It is fundamental finding for the study of subthreshold particle production, which indicates that the contribution from the high momentum component of the distribution $\Phi(q)$ might be negligible, because the available collision energy is under the production threshold. The microscopic calculations [63, 64] with realistic spectral functions confirm this expectation.

The invariant collision energy $\sqrt{s}$ of the beam proton and the target nucleon appearing in Eq.11 can be determined by analogy with Guet and Prakash [65]. The incident proton is influenced by the nuclear optical potential U, thus its total energy E_0' becomes as

$$E_0' = T_0 + m_N - U \tag{29}$$

where T_0 is the beam kinetic energy and m_N stands for the free nucleon mass. Note that the momentum of the incident proton P_0' is modified properly.

The energy E_{prod} available for the pion production is related with the incoming energy by the energy conservation rule

$$E_0' + M_A = E_{prod} + \left(M_{A-1}^2 + q^2\right)^{1/2} + E^* \tag{30}$$

with M_A and M_{A-1} being the masses of the initial and residual nuclei respectively, q is the internal momentum and E^* stands for the excitation of the final nucleus. Applying $M_{A-1} \gg q$ one can get

$$E_{prod} = E_0' + m_N - \epsilon - E^* \tag{31}$$

where ϵ is the binding energy. Minimal excitation energy E^* for almost all nuclei equals to $\simeq 1.5 - 2$ MeV. For instance the stable states of ^{11}B are below $\simeq 8$ MeV.

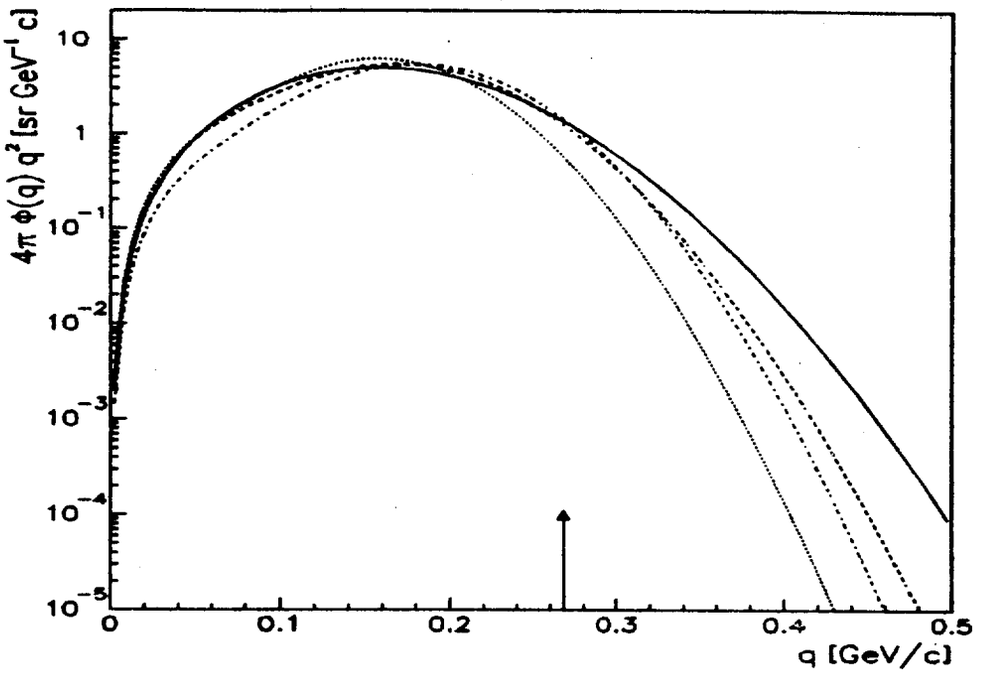

Figure 7: Nuclear momentum distributions for ^{12}C -solid, ^{40}Ca -dashed, ^{56}Fe -dotted and ^{208}Pb -dashed-dotted line. Arrow shows the Fermi momentum q_F.

However the pion production might be associated with the high energy excitation of unstable residual nuclei.

The relation between the average removal energy $\langle E \rangle$ and the excitation energy is as follows [59]

$$E^* = \langle E \rangle + M_A - M_{A-1} - m_N \tag{32}$$

which results

$$E_{prod} = E'_0 + m_N - \langle E \rangle \tag{33}$$

with mean removal energy being positive.

Therefore the invariant energy from Eq.11 is determined as

$$s = (E'_0 + m_N - \langle E \rangle)^2 - (\mathbf{P}'_0 + \mathbf{q})^2 \tag{34}$$

We adopt the momentum dependent optical potential from [66] for cold nuclear matter at normal density

$$U(p) = A + B \times \left[\frac{q_F^2 + \Lambda^2 - p^2}{2p\Lambda} \times ln \frac{(p+q_F)^2 + \Lambda^2}{(p-q_F)^2 + \Lambda^2} + \frac{2Q_F}{\Lambda} - 2\left(arctg \frac{p+q_F}{\Lambda} - arctg \frac{p-q_F}{\Lambda} \right) \right] \tag{35}$$

with $A = 30.46$ MeV, $B = -381.66$ MeV and $\Lambda = 1.58 q_F$.

Fig.8 shows the optical potential as a function of proton kinetic energy. Note that the mean field without any momentum dependence results $U \simeq -53$ MeV [67],

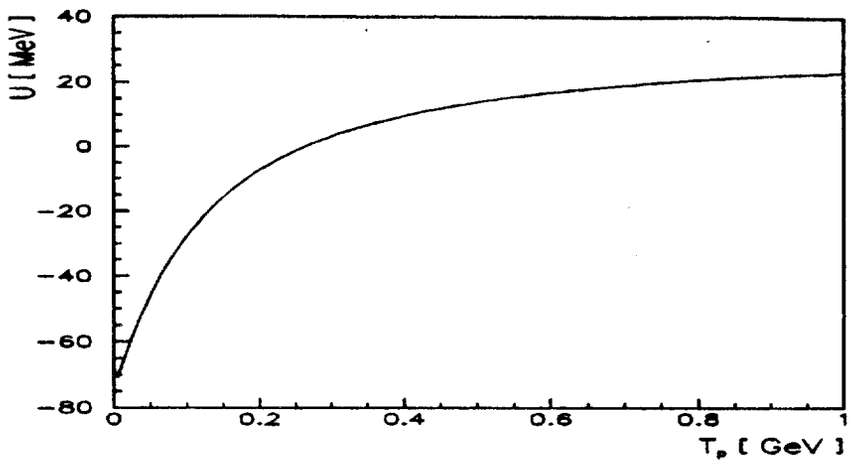

Figure 8: Optical potential as a function of the proton kinetic energy.

while the analysis of the experimental data using the Dirac equation [68, 69, 70] shows the potential becomes repulsive at energies higher than 300 MeV.

In the following calculations we use the parametrizations of the nucleon momentum distributions shown in Fig.7, which are borrowed from [61] and do not contains the high momentum part from the short-range and tensor correlations. The relation between removal energy and the nuclear momentum q was constrained with the energy sum rule (26).

7 Comparison with experimental data.

7.1 Energy dependence of the production cross section.

Fig.9 shows the total cross section of π^+-meson production from $p + A$ collisions as a function of the incident proton energy. The experimental points are taken from [71, 72], while lines are the results calculated with Eq.11.

Note that increasing the beam energy the agreement between the experimental data and the calculations for heavy targets becomes poor. We relate the discrepancy with the contribution from secondary induced reactions as

$$\begin{aligned} p + N_1 &\rightarrow \pi + N' + X \\ N' + N_2 &\rightarrow \pi' + N'' + X \\ or \;\; \pi + N_2 &\rightarrow \pi' + \pi'' + X \end{aligned} \tag{36}$$

The calculations with cascade type models, which are accounting for the secondary interactions quite reasonably reproduce the pion production at high energies [21, 23].

The beam energy dependence of π-meson production cross section from $p + C$ collisions was calculated by Guet and Prakash [65]. It was found that the calculations around 2.5 times underestimate the experimental results. The global difference

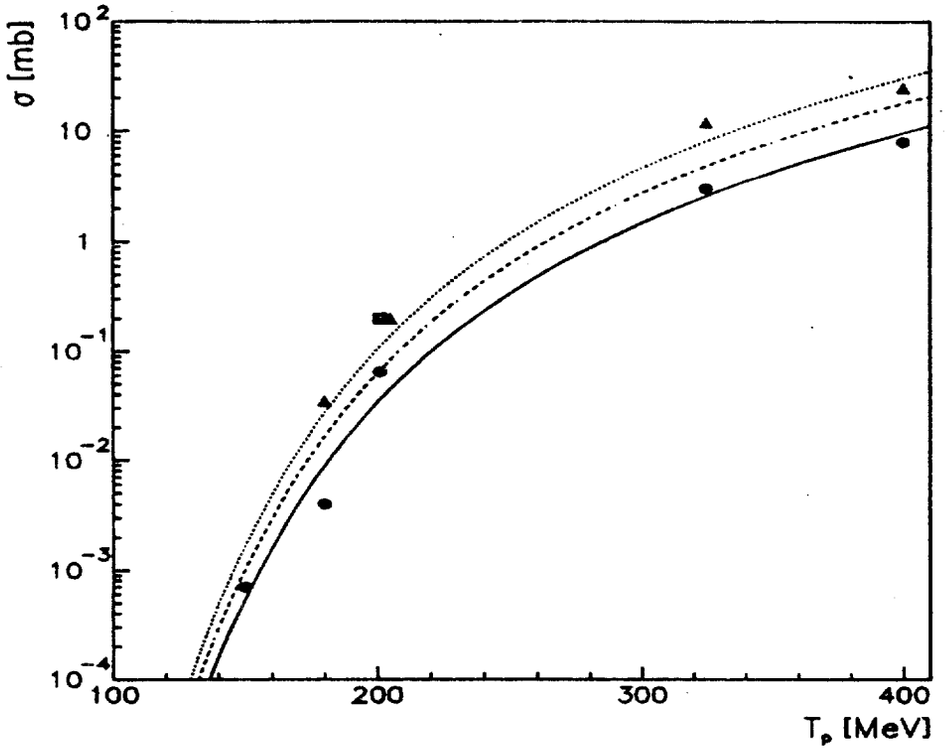

Figure 9: The cross section of π^+-meson production from $p + C$ -dots and solid, $p + Ni$ -square and dashed and $p + Pb$ collisions -triangles and dotted line as a function of the bombarding energy. Experimental points are from [71, 72] and lines show our results.

between our model and the calculations from [65] is due to the determination of the effective collision numbers. For instance, our numbers for the carbon target shown with Fig.4, as well as (21) from [43, 44] are roughly 2 times greater those from [65].

7.2 Pion production at 201 MeV

First let us to illustrate the kinematical ingredients of the calculations on pion production from $p + C$ collisions at 201 MeV. Fig.10a) shows the production cross section calculated with $\Phi(q) = const$ as a function of the momentum q and the angle Ψ between the beam proton and the nuclear nucleon in the laboratory. Obviously the contribution to the pion production comes mostly from the high internal momenta as well as from the system of the colliding beams. Fig.10b) shows the π^+-production cross section calculated with the realistic momentum distribution $\Phi(q)$ from [61].

Note that the dominant contribution comes from the momenta around 200 MeV/c, which is below the Fermi momentum. Thus the total cross section for pion production at 201 MeV is not influenced by the high momentum tail of the nuclear spectral function. Such a simple preliminary estimation prevent us from using the distribution $\Phi(q)$ containing the correlated part.

It is frequently discussed that particle production at large emission angles is sensitive to the short range correlations related with the high momentum component

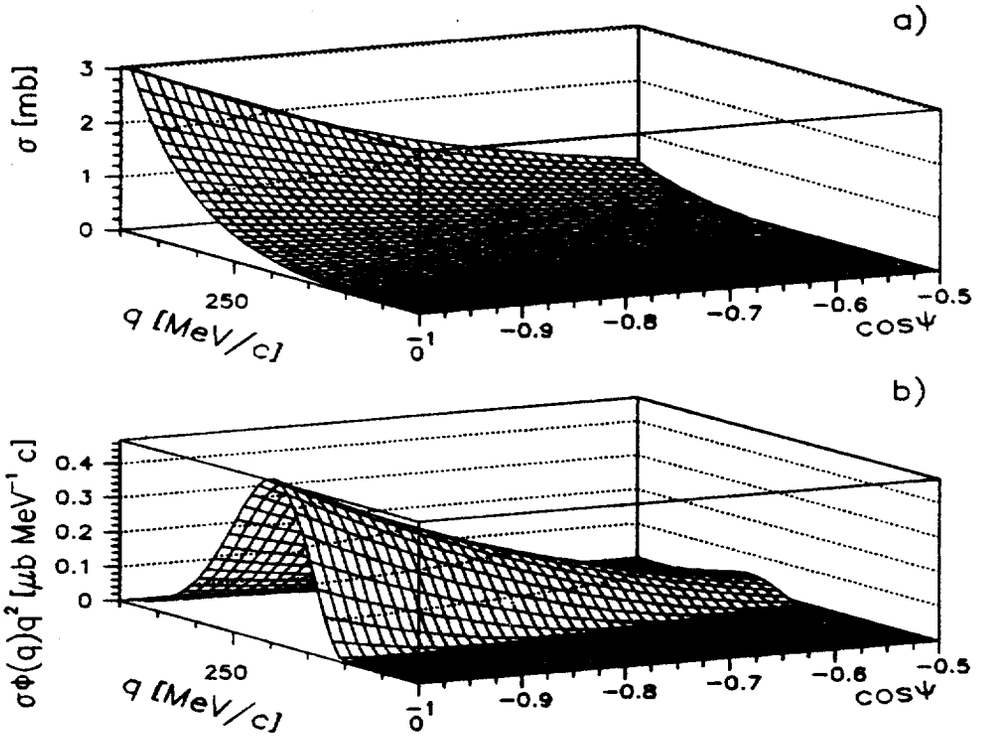

Figure 10: a) Cross section of π^+-meson production from $p + C$ collisions at 201 MeV as a function of the angle Ψ between the incident proton and target nucleon and the momentum q of the nuclear nucleon calculated with uniform momentum distribution. b) Similar as for a) calculated with realistic $\Phi(q)$.

of $\Phi(q)$. However it is not the present case. The double differential cross sections of π^+-production from $p + C$ collisions are shown with Fig.11 for the emission angles of 30° and 90° and as a function of the pion kinetic energy and momentum q.

The pions produced at emission angle $\theta = 90°$ and with energies close to the absolute kinematical threshold probe the momenta of around 300 MeV/c, which are still below the region of $q > 400$ MeV/c where the contribution from the short-range and tensor correlations becomes dominant.

Fig.12 shows the energy spectrum of π^+-mesons produced from $p + C$ collisions at 201 MeV and at emission angle of 30°. Dots are the experimental data from [71], while lines show our calculations. The peak at $T_\pi \simeq 45$ MeV is related with the deuteron production, as discussed above.

Fig.13 shows the pion spectrum for $\theta = 45°$ and also illustrates visible contribution from the quasi-deuteron reaction channel.

The energy spectra of positive pions from $p + Ni$ collisions at 201 MeV and at emission angles from 22° to 105° are shown with Fig.14,15,16. The agreement between the experimental data and our model results is quite reasonable. The discrepancy at large emission angle of $\theta = 105°$ we relate with the contribution from secondary interactions, as π^+-elastic scattering and charge-exchange reactions.

Note that due to the reaction kinematics the pion spectra from the deuteron

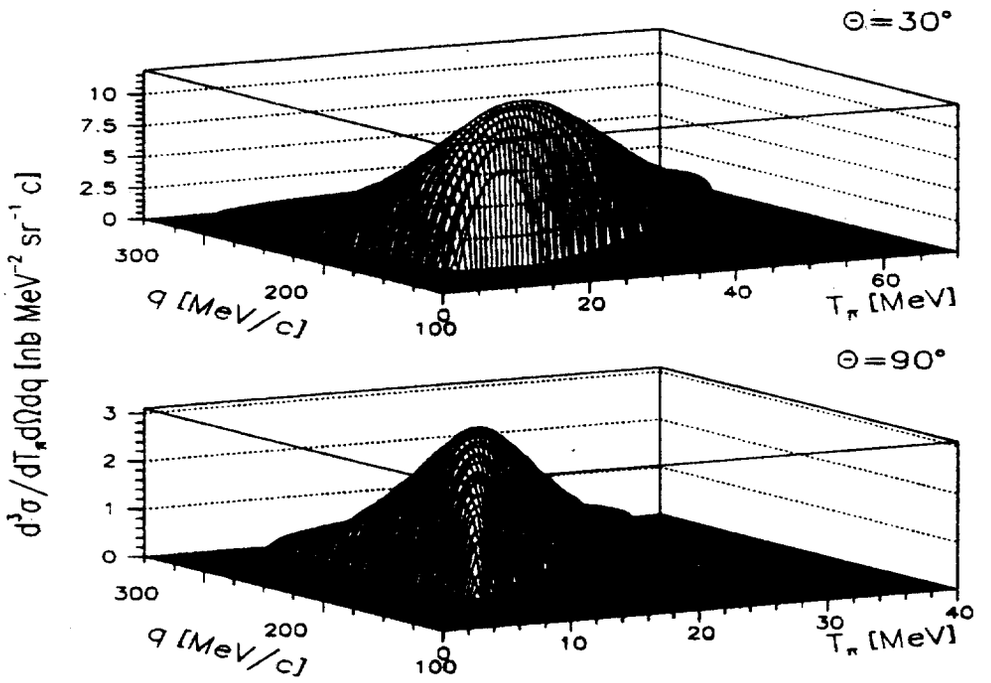

Figure 11: Cross section of π^+-production from $p + C$ collisions at bombarding energy of 201 MeV and the emission angle θ as a function of the pion kinetic energy T_π and the internal nuclear momentum q.

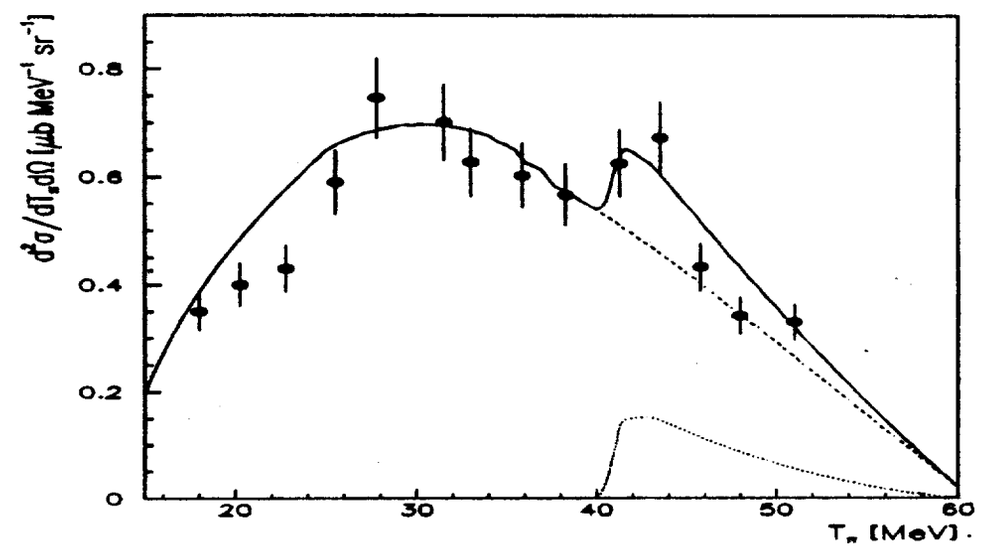

Figure 12: The energy spectrum of π^+-meson produced from $p + C$ collisions at bombarding energy of 201 MeV and detection angle of 30°. Experimental points are from [71]. Lines show the calculations. Dashed- the contribution from $p + N \rightarrow N + N + \pi^+$ and dotted from the quasi-deuteron reaction channel. Solid line shows the sum.

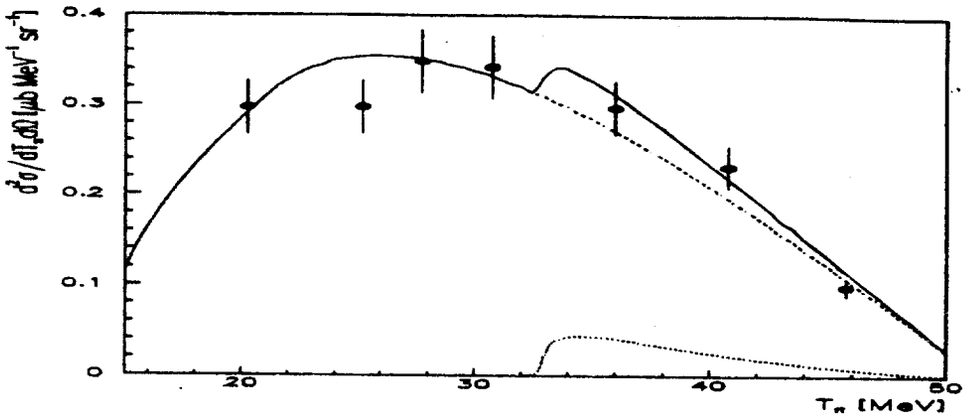

Figure 13: π^+-spectrum produced from $p + C$ collisions at 201 MeV and emission angle of 45°. The notations are similar to Fig. 12.

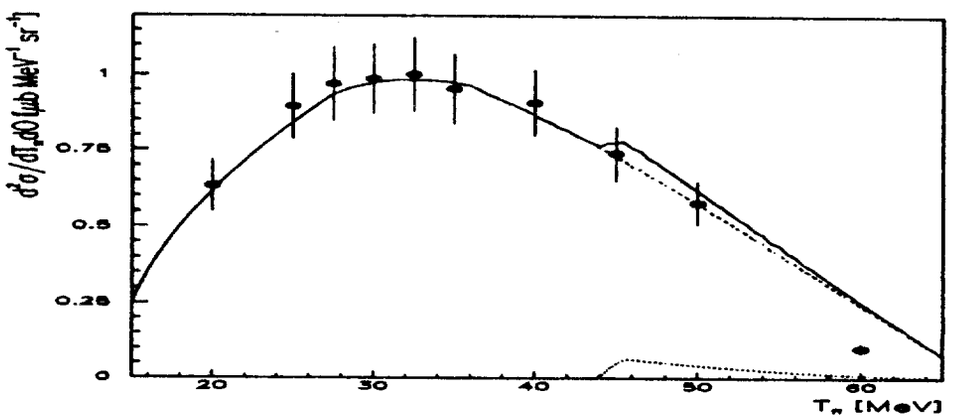

Figure 14: The energy spectrum of π^+-meson from $p + Ni$ collisions at bombarding energy of 201 MeV and emission angle of 22°. Experimental points are from [72]. Lines show the calculations. Dashed- the contribution from $p + N \to N + N + \pi^+$ and dotted from the quasi-deuteron reaction channel. Solid line is the sum.

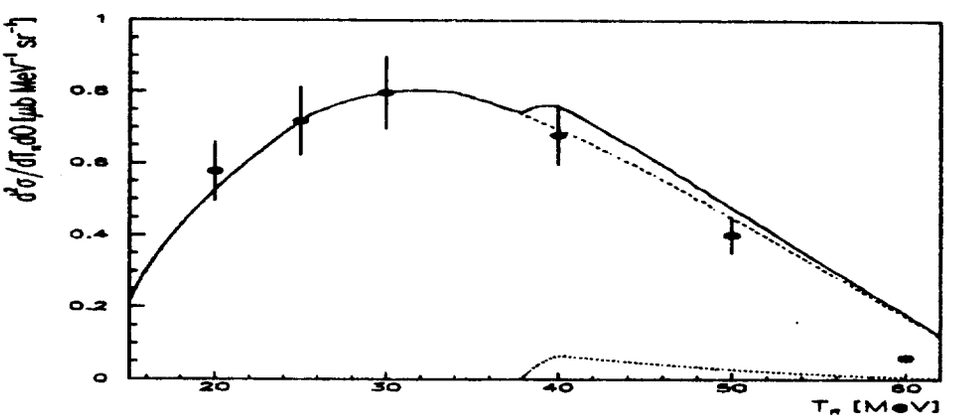

Figure 15: Energy spectrum of π^+-meson from $p + Ni$ collisions at bombarding energy of 201 MeV and emission angle of 35°. The notations are similar to Fig. 14.

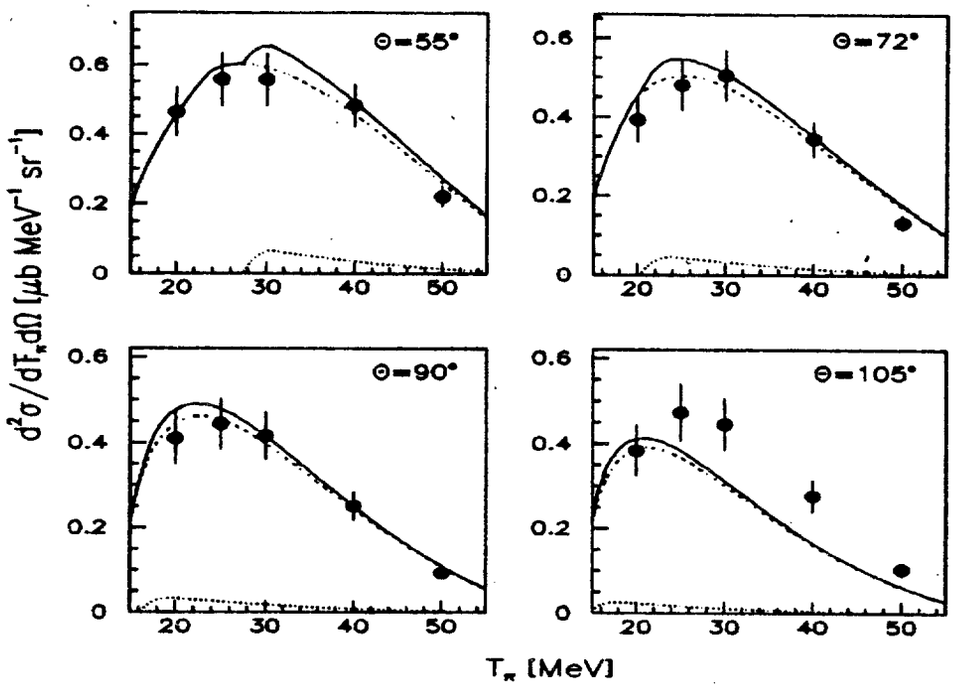

Figure 16: Energy spectra of π^+-meson from $p+Ni$ collisions at bombarding energy of 201 MeV and the emission angle θ. The notations are similar to Fig. 14.

channel are shifted to lower energies with increasing the detection angle. The quasi-deuteron peak also exist at large emission angles but can not be observed being dissolved with the contribution from $p + N \to N + N + \pi^+$ reaction channel.

Fig.17 shows the angular spectra of π^+-mesons produced from $p + Ni$ collisions at 201 MeV and for the pion energies of 30, 40 and 50 MeV.

Let us to analyze the experimental data. The pion angular spectra might be subdivided by two parts, as are shown with the dashed lines. First one is the forward peaked angular distribution with a slope rather independent on the pion kinetic energy. We relate this part with the direct pion production as discussed within the present model. The nature of a forward peaked distribution is in accord with the Lorentz boost of spectra in the laboratory system, i.e. due to the kinematical reason only. We fairly reproduce this part of the pion angular spectra.

Second part indicates almost isotropical distribution, which can not be obtained with applying of the direct production mechanism. We are referring this part to the secondary interactions as pion rescattering in nuclear medium. Indeed, the produced pions are slow and scatter as

$$\pi + N \to \pi' + N' \tag{37}$$

in s-wave [73], i.e. isotropically in the rest system of the residual nucleus, which is almost the laboratory system because the recoil momentum is small. The pion-nucleon scattering populates all emission angle. However its contribution to the forward angles is almost negligible for π^+-production and high pion energies, because of the strong contribution from the direct reactions (6,7).

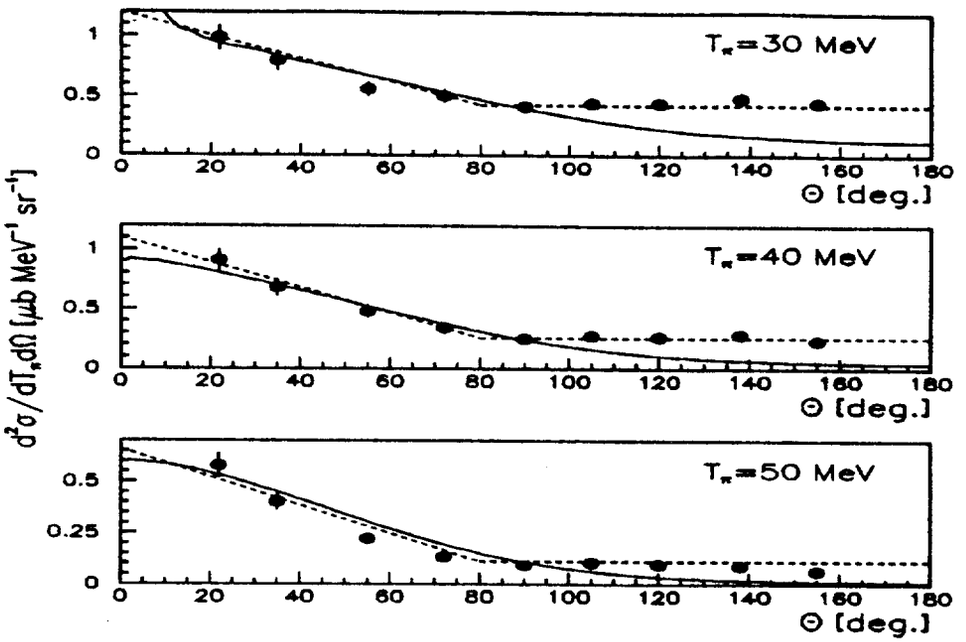

Figure 17: Angular spectra of π^+-meson from $p+Ni$ collisions at bombarding energy of 201 MeV and pion kinetic energy T_π. Experimental points are from [72]. Solid lines show the contribution from $p + N \to N + N + \pi^+$ channel. The dashed lines indicate the contributions from primary and secondary interactions.

As opposed to the π^+-mesons, the negative pions are produced roughly equally from the direct reaction mechanism as well as from the secondary charge-exchange scattering. We discussed this opportunity in the section on elementary production cross section. Therefore the angular spectrum of π^--mesons might show flat distribution. Moreover the spectra become mostly isotropical for the heavy targets, when the secondary interactions are probable.

The energy spectra of π-mesons produced from $p+Ni$ collisions at 201 MeV are shown in Fig.18,19 for the detection angles from 22° to 105°.

The model rather well reproduces the spectra at angles less than 72°, while substantially underestimates the π^--production cross sections at large angles. Note that experimental results from Fig.18,19 indicate almost isotropical angular distribution at $\theta \geq 35°$. Within the present approach we are failed to describe the π^--spectra, because the model does not account for the secondary interactions.

Let us to prevent from the expectation that with increase of the beam energy the π^--angular spectra might be isotropical. At high collision energy the produced pions are relatively fast. The angular distribution of $\pi+N$ scattering at the Δ-isobar region is described as

$$d\sigma/d\Omega \propto 1 + 3cos^2\theta \tag{38}$$

with θ being the pion emission angle in the $\pi + N$ center of mass system. For much higher pion energies the angular spectrum is strongly forward peaked. As an additional factor the Lorentz boost for the $\pi + N$ scattering is always valid.

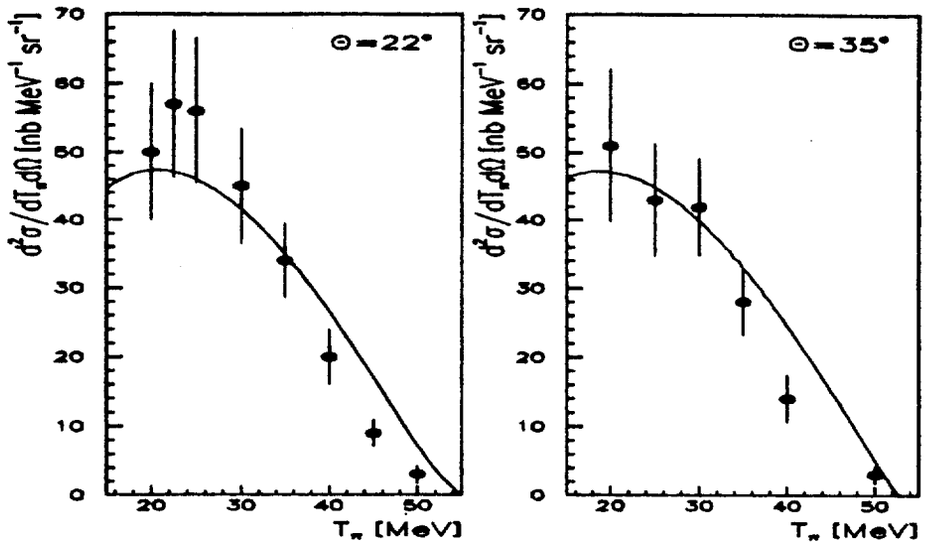

Figure 18: Energy spectra of π^--meson from $p+Ni$ collisions at bombarding energy of 201 MeV and the emission angle θ. Experimental points are from [72]. Lines show the contribution from $p+n \to p+p+\pi^-$ reaction channel.

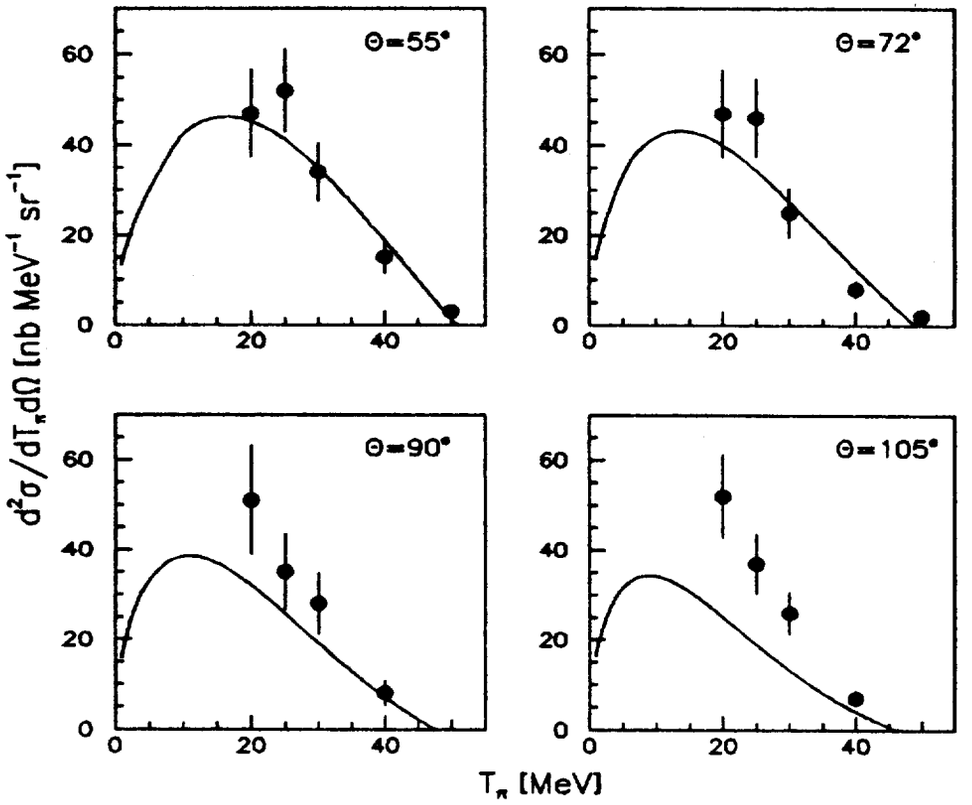

Figure 19: Energy spectra of π^--meson from $p+Ni$ collisions at bombarding energy of 201 MeV and the emission angle θ. The notations are similar to Fig. 18.

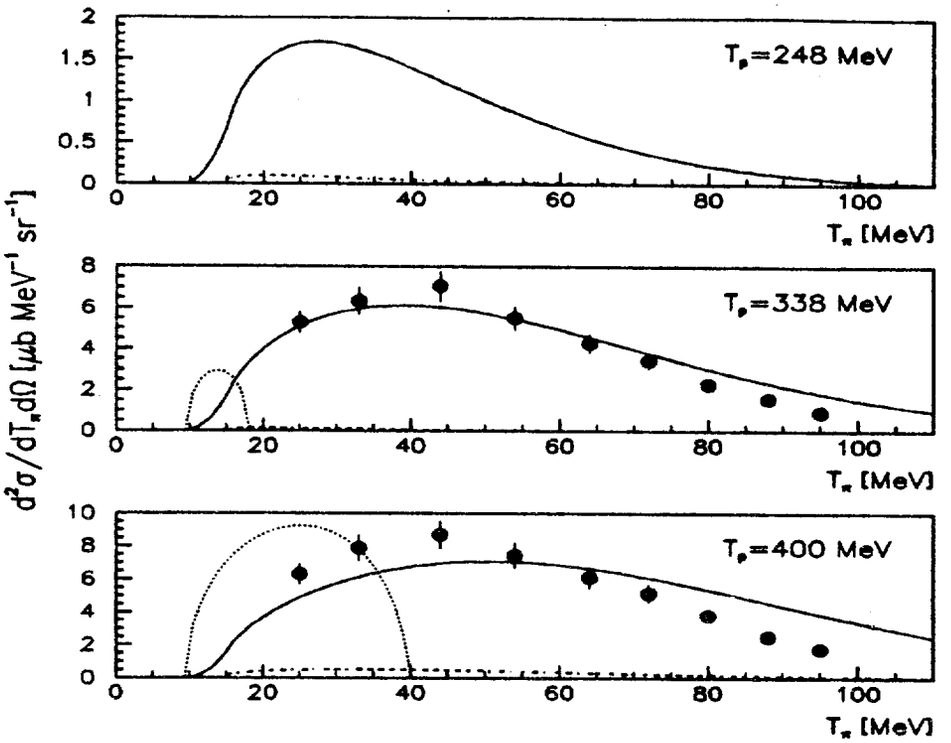

Figure 20: Energy spectra of π^+-meson produced from $p + Cu$ collisions at emission angle of 90° and bombarding energy T_p. Experimental points are from [74]. Solid lines show the contribution from $p + N \to N + N + \pi^+$ and dashed- from the quasi-deuteron reaction. Dotted lines show the pion spectra from $p + N$ collision in free space.

7.3 Pion production above the threshold.

To illustrate the reliability of the present approach at high energies we calculate the pion production at 338 and 400 MeV and compare our results with the experimental data. Fig.20 shows the energy spectra of positive pions produced from $p + Cu$ collisions and at emission angle of 90°. The experimental data are taken from [74]. The solid lines show the calculations with (11) accounting for the three body final state, while the dashed lines are the contribution from the quasi-deuteron channel.

The dotted lines show the calculation on π^+-meson production from the collision of beam proton with free nucleon, i.e. assuming $\Phi(q) = 0$. Note that we do not perform the calculations in free space for the beam energy of 248 MeV, which is below the pion production threshold. The results from Fig.20 illustrate the importance of the internal momentum distribution for the calculations of meson production also above the reaction threshold. The influence of the $\Phi(q)$ on the shape of the pion spectrum is apparent.

As a prediction of the model Fig.21 shows π^+ and π^--meson spectra produced from $p + Cu$ collision at 248 MeV and detection angle $\theta = 22°$. Because of the reaction kinematics the peak from the quasi-deuteron reaction mechanism is dissolved by the contribution from $p + N \to \Delta + N \to N + N + \pi^+$ channel. Remind that

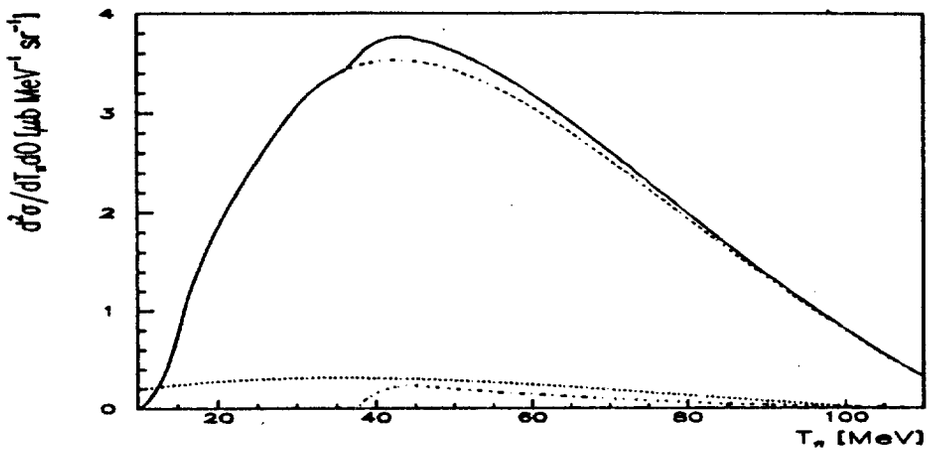

Figure 21: Pion energy spectra from $p + Cu$ collisions at bombarding energy of 248 MeV and emission angle of 32°. Dashed line shows the contribution from $p + N \rightarrow N + N + \pi^+$, dotted- $p + n \rightarrow p + p + \pi^-$ and dashed-dotted- from the quasi-deuteron reaction channel. Solid line is the total π^+-spectrum.

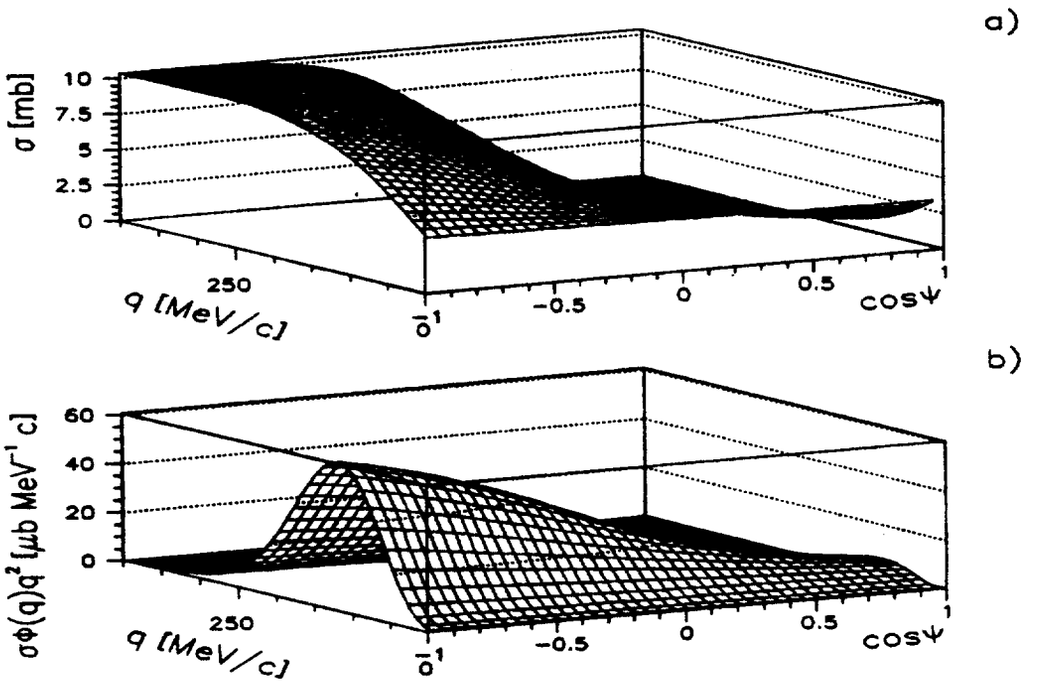

Figure 22: a) Cross section of π^+-meson production from $p + C$ collisions at 585 MeV as a function of the angle Ψ between the beam proton and target nucleon and the momentum q calculated with $\Phi(q) = const.$ b) Similar as for a) calculated with $\Phi(q)$ from [61].

at beam energy of 201 MeV the π^+-spectra at forward angles perform transparent quasi-deuteron peak.

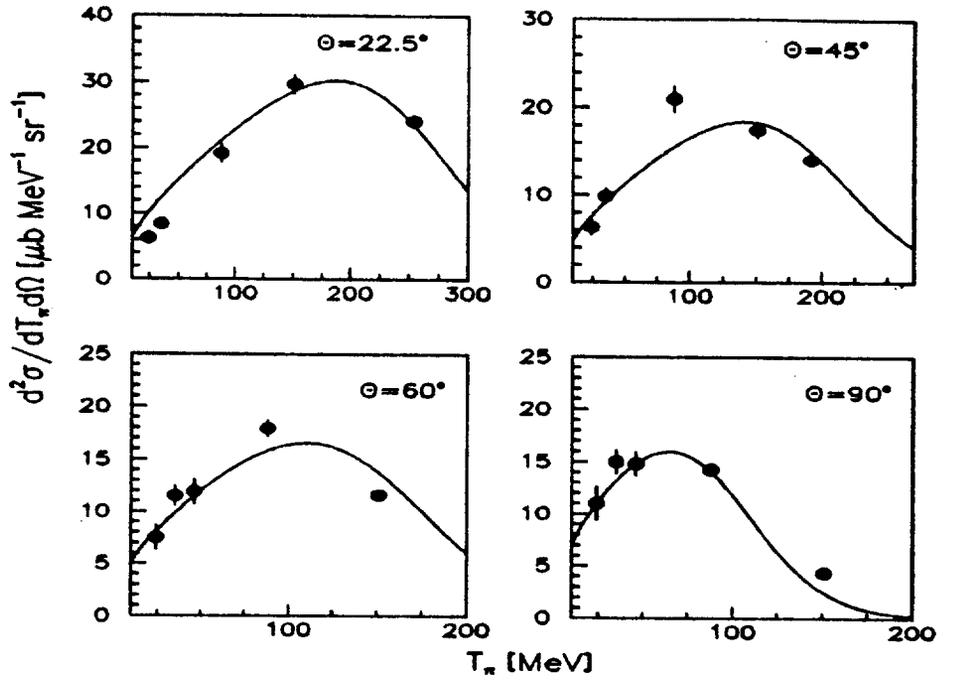

Figure 23: Energy spectra of π^+-meson from $p+C$ collisions at bombarding energy of 585 MeV and the emission angle θ. Experimental points are from [75]. Lines show the model results.

The kinematical constraints of the pion production from $p + C$ collisions at such high beam energy as 585 MeV are shown with Fig.22. Fig.22a) performs the production cross section calculated with $\Phi(q) = const$ as a function of the momentum q and the angle Ψ between the beam proton and the target nucleon in the laboratory. Fig.22b) shows the π^+-production cross section calculated with the carbon momentum distribution from [61].

The dominant contribution to π^+-meson production cross section comes from the internal momenta as close to 150 MeV/c, which is almost twice below the Fermi level. Thus already above the pion production threshold one can trust the reliability of the cascade type models adopting the mean field approach, i.e. assuming that individual nucleons move as independent particles in an average potential.

The energy spectra of π^+-mesons produced from $p+Cu$ collisions at 585 MeV are shown in Fig.23 for the pion emission angles from 22.5° to 90°. The experimental data were taken from [75]. The agreement between the model and experimental results is reasonable. Note that the energy spectra of pions overlap with the Δ-isobar region as is shown with Fig.3 and therefore proposing the strong final state interaction.

Fig.24 shows π^--spectra from $p + Cu$ collisions at 585 MeV. The model underestimates the cross sections for low energy π^--mesons, which again indicate the possible contribution from the secondary charge-exchange pion rescattering. Again the high energy pions are reasonably reproduced.

Indeed, at high collision energies the high energy pions are predominately produ-

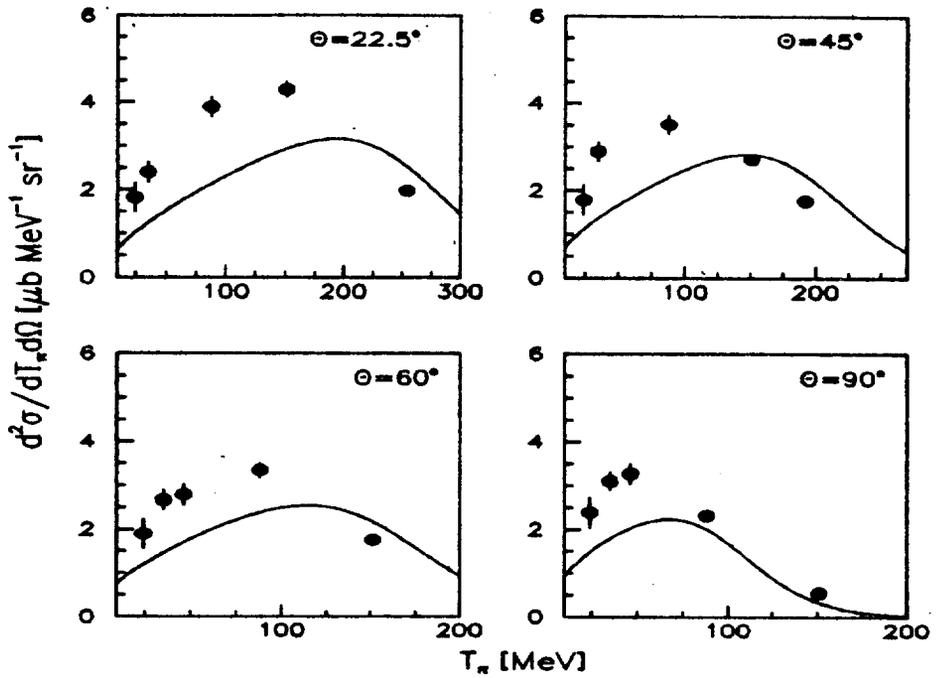

Figure 24: Energy spectra of π^--meson from $p+C$ collisions at bombarding energy of 585 MeV. Notations are similar to Fig.23.

ced from primary reactions, while soft pions from secondary one. As an additional indication, the pions at such high energies are scattered through the Δ-excitation following the forward-angles anisotropy as (38). Thus the contribution from pion rescattering to the forward detection angles becomes dominant. As a result we observe a strong discrepancies at angles of 22.5° and 45°, while the cross sections of π^--production at 60° and 90° are described much better.

8 Conclusions.

Within the single particle approximation we perform the study on subthreshold pion production from proton-nucleus collisions. To calculate the direct production mechanism we adopt the on-shell elementary cross sections and the isobar model. The deuteron channel was considered as applying the deuteron formation outside the nucleus in accord with the coalescence mechanism.

The pion production and distortion in nuclear medium were provided with the Glauber formalism. We use the nuclear momentum distributions from realistic model on the nuclear spectral function and follow the relation between the internal nuclear momenta and the energies of the bounds nucleons using the Koltun sum rule.

It was found that the spectra of π^+-mesons from $p+A$ collisions at 201 MeV are fairly well reproduced with the model calculations. It was shown that the structure observed from π^+-spectra at forward angles is related to the quasi-deuteron production mechanism. However the calculations strongly underestimate the cross sections

of π^--meson production.

In order to study while the discrepancy is influenced by the subthreshold phenomena we perform the analysis of pion production above the free nucleon-nucleon reaction threshold. The differential cross section of π^+-production are well described by the model, while those for π^--mesons are not.

Thus we conclude that the difference between the experimental cross section of π^--meson production from $p + A$ collisions and the model results is not connected with the beam energy or the effects of the subthreshold pion production.

We associate the discrepancy with the contribution from the secondary interactions of pions in the nuclear environment. Such pion rescatterings are important for the negative pion production due to the elementary nucleon-nucleon production cross sections and the $\pi + N \rightarrow \pi + N$ kinematics.

It was found no crucial arguments for the incorporation of the reaction mechanisms beyond the standard in order to get a better description of the experimental data.

9 Acknowledgments.

I gratefully acknowledge A.Badala, R.Barbera, A.Palmeri, G.S.Pappalardo and F.Riggi for the cooperation and many fruitful discussions concerning the analysis of the experimental data and for warm hospitality during my stay in Catania. Thanks are also due to A.Bonasera and M.DiToro for the enlightening remarks. I appreciate the discussions with J.Cugnon and suggestions concerning the application of the isobar model. I would like to thank W.Cassing for the helpful remarks and his attention to the importance of the secondary interactions for the negative pion production.

The work is partly supported by Istituto Nazionale di Fisica Nucleare, Sezione di Catania and Physics Department of University of Catania.

References

[1] G. Bertsch and S.Das Gupta *Phys. Rep.* **160** (1988) 189.

[2] K. Klingenbeck, M. Dillig and M.G. Huber *Phys. Rev. Lett.* **47** (1981) 1655.

[3] V. Metag *Prog. Part. Nucl. Phys.* **30** (1993) 75.

[4] A. Bonaseral, F. Gulminelli and J.J. Molitoris *Phys. Rep.* **243** (1994) 1.

[5] P. Grimm and E. Grosse *Prog. in Part. and Nucl. Phys.* **15** (1985) 339.

[6] E. Grosse *Nucl. Phys.* **A447** (1986) 611.

[7] R.J. Glauber and G. Mattia *Nucl.Phys.* **B21** (1970) 135.

[8] G. Bertsch *Phys. Rev.* **C15** (1977) 713.

[9] J. Cugnon, D. Kinet and J. Vandermeulen *Nucl. Phys.* **A379** (1982) 553.

[10] B.J. VerWest and R.A. Arndt *Phys. Rev.* **C24** (1982) 1979.

[11] M. Büscher, A.A. Sibirtsev and K. Sistemich *Z. Phys.* **A350** (1994) 161.

[12] G.A. Lobov and A.A. Sibirtsev *Sov. J. Nucl. Phys.* **52** (1990) 1077.

[13] P.C. Gugelot and S.M. Paul *Z. Phys.* **A344** (1993) 325.

[14] I.A. Vorontsov et al. *Preprint ITEP* **ITEP-144** (1984)

[15] A.A. Cowley and P.G. Roos *Phys. Rev.* **C45** (1992) 1745.

[16] W. Cassing *Private communication*

[17] A.K. Kerman, H.Mc Manus and R.M. Thaler *Annals of Phys.* **8** (1959) 55.

[18] R.G. Newton *Scattering Theory of Waves and Particles* New York, McCraw-Hill (1966).

[19] D.F. Jackson *Nuclear Reactions* London, Methuen (1970).

[20] G.R. Satchler *Introduction to Nuclear Reactions* Hong Kong, Macmillan Education LTD (1990)

[21] W. Cassing et al., *Phys. Rep.* **188** (1990) 363.

[22] A.A. Sibirtsev, *Phys. Scr.* **RS21** (1993) 167.

[23] J. Cugnon and M.-C. Lemaire *Nucl. Phys.* **A489** (1988) 781.

[24] A. Sibirtsev, K. Tsushima and A. Faessler *Z. Phys.* **A354** (1996) 215.

[25] A.A. Sibirtsev et al. *Yad. Fiz.* **42** (1985) 482.

[26] C. Ellegard et al.*Phys. Rev. Lett.* **50** (1983) 1745.

[27] D. Contardo et al. *Phys. Let.* **B168** (1986) 331.

[28] C. Gaarde *Nucl. Phys.* **A478** (1988) 475.

[29] M. Trzaska et al. *Z. Phys.* **A340** (1991) 325.

[30] J. Cugnon *Private communication*

[31] A.A. Sibirtsev et al. *Z. Phys.* **A347** (1994) 277.

[32] R. Machleidt, K. Holinde and C. Elster *Phys. Rep.* **149** (1987) 1.

[33] G. Bertsch and J. Cugnon *Phys. Rev.* **C24** (1981) 2514.

[34] A. Moalem et al. *hep-ph/9505264* (1995)

[35] S.T. Butler and C.A. Pearson *Phys. Rev.* **129** (1962) 836.

[36] B. Margolis *Phys. Lett.* **B26** (1968) 524.

[37] E. Vercellin et al. *Nuovo Cim.* **A106** (1993) 861.

[38] J. Knoll and J. Randrup *Nucl. Phys.* **A324** (1979) 445.

[39] W. Zwermann and B. Schürmann *Phys. Lett.* **B145** (1984) 315.

[40] C.M. Ko *Phys. Lett.* **B138** (1984) 361.

[41] H.W. Barz and H. Iwe *Phys. Lett.* **B153** (1985) 217.

[42] A. Sibirtsev et al. *Z. Phys.* **A351** (1995) 333.

[43] W. Cassing et al. *Phys. Lett.* **B238** (1990) 25.

[44] A. Sibirtsev and M. Büscher *Z. Phys* **A347** (1994) 191.

[45] V. Bellini et al. *Z. Phys.* **A333** (1989) 393.

[46] K.G.R. Doss and W.R. Wharton *Phys. Rev.* **C22** (1980) 1219.

[47] D.O. Riska and H. Sarafian *Phys. Rev.* **C22** (1980) 1222.

[48] A. Badala et al., *Phys. Rev.* **C43** (1991) 190.

[49] E. Segre *Nuclei and Particles* The Benjamin/Cummings Publishing Company (1977).

[50] S. Fantoni and V.R. Pandharipande *Nucl. Phys.* **A427** (1984) 473.

[51] O. Benhar, A. Fabrocini and S. Fantoni *Nucl. Phys.* **A550** (1992) 201.

[52] O. Benhar, A. Fabrocini and S. Fantoni *Nucl. Phys.* **A505** (1989) 267.

[53] C. Mahaux and R. Sartor *Nucl. Phys.* **A546** (1992) 65.

[54] M. Baldo et al. *Nucl. Phys.* **A545** (1992) 741.

[55] C. Ciofi degli Atti, E. Pace and G. Salme *Phys. Rev.* **C21** (1980) 805

[56] P. Fernandez de Cordoba and E. Oset *Phys. Rev.* **C46** (1992) 1697

[57] P. Fernandez de Cordoba et al. *nucl-th/9511038* (1995)

[58] D.S. Koltun *Phys. Rev.* **C9** (1974) 484.

[59] S.Frullani and J.Mougey, *Advances in Nucl. Phys.* **14** (1984) 7.

[60] P.K.A. De Witt Huberts *J. of Phys.* **G16** (1990) 507.

[61] C. Ciofi degli Atti and S. Simula *Phys. Rev.* **C53** (1996) 1689.

[62] C. Ciofi degli Atti, E. Pace and G. Salme *Phys. Lett.* **B141** (1984) 14.

[63] M. Debowski, E. Grosse and P. Senger *GSI report* **GSI 10-95** (1995) 3.

[64] W. Cassing *Private communication*

[65] C. Guet and M. Prakash *Nucl. Phys.* **A428** (1984) 119.

[66] G.M. Welke et al. *Phys. Rev.* **C38** (1988) 2101.

[67] G.F. Bertsch, H. Kruse and S. Das Gupta *Phys. Rev.* **C29** (1984) 673

[68] K. Weber et al. *Nucl. Phys.* **A552** (1993) 571.

[69] E.D. Cooper *Phys. Rev.* **C36** (1987) 2170.

[70] S. Hama et al. *Phys. Rev.* **C41** (1990) 2737.

[71] L. Bimbot et al., *Nucl. Phys.* **A440** (1985) 636.

[72] A. Badala et al. *Phys. Rev.* **C46** (1992) 604.

[73] Landolt-Börstein *New Series, ed H. Schopper* **I/12** (1988).

[74] J.Julien et al. *Phys. Lett.* **B142** (1984) 340.

[75] J.F.Crawford et al. *Phys. Rev.* **C22** (1980) 1184.